Nuclear spin selective laser control of rotational and torsional dynamics

J. Floß, T. Grohmann, M. Leibscher, and T. Seideman

Citation: The Journal of Chemical Physics **136**, 084309 (2012); doi: 10.1063/1.3687343
View online: http://dx.doi.org/10.1063/1.3687343
View Table of Contents: http://scitation.aip.org/content/aip/journal/jcp/136/8?ver=pdfcov
Published by the AIP Publishing

Nuclear spin selective laser control of rotational and torsional dynamics

J. Floß,[1,2] T. Grohmann,[2] M. Leibscher,[2,a)] and T. Seideman[3]
[1]*Department of Chemical Physics, The Weizmann Institute of Science, Rehovot 76100, Israel*
[2]*Institut für Chemie und Biochemie, Freie Universität Berlin, Takustr. 3, 14195 Berlin, Germany*
[3]*Department of Chemistry, Northwestern University, 2145 Sheridan Rd, Evanston, Illinois 60208, USA*

(Received 22 November 2011; accepted 2 February 2012; published online 28 February 2012)

We explore the possibility of controlling rotational-torsional dynamics of non-rigid molecules with strong, non-resonant laser pulses and demonstrate that transient, laser-induced torsional alignment depends on the nuclear spin of the molecule. Consequently, nuclear spin isomers can be manipulated selectively by a sequence of time-delayed laser pulses. We show that two pulses with different polarization directions can induce either overall rotation or internal torsion, depending on the nuclear spin. Nuclear spin selective control of the angular momentum distribution may open new ways to separate and explore nuclear spin isomers of polyatomic molecules. © *2012 American Institute of Physics*. [http://dx.doi.org/10.1063/1.3687343]

I. INTRODUCTION

The rotations of molecules can be effectively controlled by moderately intense laser pulses, employing interaction of the field with the permanent or the induced dipole of the molecule. Molecular alignment, in particular, has been studied intensively during the past few years due to its numerous applications, ranging from chemical reaction dynamics to high harmonic generation. If the laser field is turned on and off adiabatically, the alignment disappears once the field is turned off. Field-free alignment can be created with short laser pulses (short with respect to the molecular rotational periods).[1] Here, the laser pulse excites rotationally broad wavepackets, where the phase relations among the rotational components guarantee that the molecule will align with the polarization vector(s) after the end of the pulse, subsequently exhibiting (coherent) dephasing, due to the unequal rotational level spacings. As a result of the phenomenon of quantum revivals, the early time alignment is fully or partially reconstructed after turn-off of the pulse, under field-free conditions. In the case of linear and symmetric top molecules, the initial alignment is precisely reproduced periodically in time, as long as coherence is maintained. The application of a pair of pulses to induce unidirectional rotation about a molecular axis has been also demonstrated, both theoretically[2–5] and experimentally.[2,3,6]

The ability to control molecular alignment can be employed to selectively manipulate chemically close species. An example is nuclear spin modifications: molecules with identical nuclei can occur in the form of nuclear spin isomers, differing by the symmetry of their nuclear spin states. The most familiar example of nuclear spin isomers is para- and ortho-hydrogen,[7] but also polyatomic molecules can have different nuclear spin modifications. Here, the separation and conversion of the isomers is still a challenge and has been performed for only few species.[8–10] The symmetrization postulate, or Pauli's principle, implies that the symmetry of the nuclear spin determines the symmetry of the spatial molecular wavefunction, in particular rotational and torsional wavefunctions. Rotational dynamics thus depend on the nuclear spin of the molecules; it has been observed that at specific times after the alignment pulse the molecules belonging to one isomer are aligned along the polarization direction of the field, while the molecules belonging to the second isomer are anti-aligned.[11] These differences in the rotational dynamics can be used to selectively manipulate the nuclear spin isomers by subsequent, properly time-delayed, laser pulses.[11–13] In polyatomic molecules, more than two nuclear spin isomers can exist. In Ref. 14, it is shown that the four nuclear spin isomers of ethylene can all be distinguished by their rotational dynamics. Controlling molecular alignment thus offers a new route for the separation of nuclear spin isomers.

Moderately intense laser pulses, which have proven powerful in steering rotational dynamics, can also be applied to control internal dynamics in molecules. The branching ratio of photo-dissociation in IBr has been controlled by strong non-resonant laser pulses,[15] and the use of Stark shifts to control radiation-less decay through conical intersections was proposed.[16] The application of moderately intense laser pulses to control internal torsion has been proposed in Ref. 17 and realized experimentally in Refs. 18 and 19. Numerous applications of controlling torsional dynamics by strong laser fields are discussed in Refs. 17 and 20, ranging from control of charge transfer reactions and purification of thermal racemates, to field guided molecular assembly and optical control of electron dynamics in molecular junctions.[20]

In this study, we investigate nuclear spin selective effects of laser controlled torsion. It has been shown previously that photo-induced intramolecular torsion can be nuclear spin selective.[21,22] Here, we propose a simple model for the description of intra-molecular torsion in the electronic ground state, induced by non-resonant laser pulses, and investigate the prospects of inducing torsional alignment (Sec. II). We then demonstrate that transient molecular torsion is sensitive to the nuclear spin of the molecules (Sec. III). In Sec. IV, we show that nuclear spin selective uni-directional rotation and

a)Author to whom correspondence should be addressed. Electronic mail: monika.leibscher@chemie.fu-berlin.de.

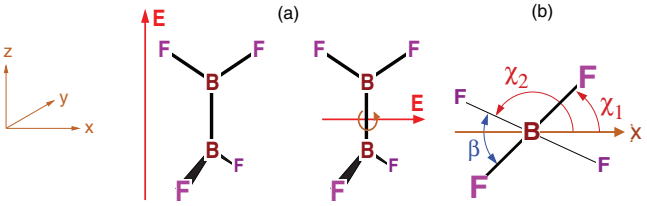

FIG. 1. (a) Torsional alignment: A first pulse aligns the major molecular axis along the space-fixed z axis. A second, short pulse, polarized perpendicular to the z axis, induces intra-molecular torsion. (b) Coordinate system using diboron tetrafluoride as an example.

torsion can be excited by a sequence of laser pulses and in Sec. V we conclude, with a discussion of the prospects for nuclear spin selective manipulation of non-rigid molecules.

II. TORSIONAL ALIGNMENT OF NON-RIGID MOLECULES

In order to investigate how intra-molecular torsion is influenced by strong, non-resonant laser pulses, we consider molecules where two parts of the system can rotate against each other because they posses a low torsional barrier. Examples are biphenyls[17–19] or molecules such as B_2F_4 or B_2Cl_4.[24–26] We envision a two-pulse scenario, where a first linearly polarized pulse aligns the major molecular axis and a second pulse, linearly polarized perpendicular to the first one, excites intra-molecular torsion as well as rotation perpendicular to the molecular axis (see Fig. 1). Here, we assume that the molecules are already (perfectly) aligned along the space-fixed z axis and investigate the effects of a short x-polarized laser pulse. (A similar model has been employed in Ref. 19.) The rotation of the two parts of the molecule can then be expressed by the Hamiltonian

$$\hat{H}_{mol} = -\frac{\hbar^2}{2I_1}\frac{\partial^2}{\partial\chi_1^2} - \frac{\hbar^2}{2I_2}\frac{\partial^2}{\partial\chi_2^2} + V(\chi_1 - \chi_2), \tag{1}$$

where I_1 and I_2 are the moments of inertia and χ_1 and χ_2 are the rotational angles of the individual parts of the molecules, as defined in Fig. 1. The torsional potential is denoted by $V(\chi_1 - \chi_2)$. If the two parts of the molecule have the same moments of inertia $I_1 = I_2 = I$, one can introduce the torsion angle $\beta = \chi_1 - \chi_2$ and the rotation angle $\chi = (\chi_1 + \chi_2)/2$ to separate the Hamiltonian into a rotational and a torsional part,[17,23]

$$\hat{H}_{mol} = \hat{H}_{rot} + \hat{H}_{tor} = -\frac{\hbar^2}{2I_{tot}}\frac{\partial^2}{\partial\chi^2} - \frac{\hbar^2}{2I_{red}}\frac{\partial^2}{\partial\beta^2} + V(\beta) \tag{2}$$

with $I_{tot} = 2I$ being the total moment of inertia and with $I_{red} = I/2$ being the reduced moment of inertia. In the following, we will use the dimensionless parameters $E' = E/E_{tor}$ with $E_{tor} = \hbar^2/I_{red}$ for the energy and $\tau = t/t_0$, with $t_0 = I_{red}/\hbar$ for the time. For B_2F_4, for example, $E_{tor} = 1.69 \times 10^{-4}$ eV and $t_0 = 12.2$ ps. The eigenfunctions $\phi_k^{rot}(\chi)$ of the rotational Hamiltonian are plane waves with the corresponding eigenvalues $E_k^{rot} = \frac{1}{2}\frac{I_{red}}{I_{tot}}k^2 = \frac{k^2}{8}$. For the torsional part of the Hamiltonian, we assume a simple periodic model for the potential

$$V = \frac{V_0}{2}\cos(2\beta) + \frac{|V_0|}{2}, \tag{3}$$

where $|V_0|$ is the barrier height. A barrier with $V_0 > 0$ corresponds to a potential with a maximum at $\beta = 0$ and a minimum at $\beta = \pi/2$, i.e., the molecule is twisted in its equilibrium configuration (such as B_2Cl_4); $V_0 < 0$, on the other hand, has a minimum at $\beta = 0$ and, therefore, describes molecules which have a planar equilibrium structure, such as B_2F_4. The eigenfunctions $\phi_n^{tor}(\beta)$ of the torsional Hamiltonian are the Mathieu functions,[27,28] and the energy eigenvalues $E_n^{tor} = (a_n(V_0) + |V_0|)/2$ are the scaled characteristic values of the Mathieu functions.

In order to model the interaction between a laser pulse and the molecules, it is assumed that both parts of the molecule will interact independently with the laser field. This assumption is valid if the interaction between the two parts is small.[17,29] The interaction with the field can then be written as

$$\hat{H}_{int} = \hat{H}_{int}^{(1)} + \hat{H}_{int}^{(2)} \tag{4}$$

with[1]

$$\hat{H}_{int}^{(j)} = -\frac{\varepsilon^2(\tau)}{4}\frac{\Delta\alpha_j}{E_{tor}}\cos^2\chi_j + C_j \tag{5}$$

and $j = 1, 2$, where $\varepsilon^2(\tau)$ is the envelope of the laser pulse, $\Delta\alpha_j = \alpha_{xx}^{(j)} - \alpha_{yy}^{(j)}$ is the polarizability anisotropy, and C_j is a constant which can and will be neglected in the following. For molecules having two identical parts, $\Delta\alpha_1 = \Delta\alpha_2 = \Delta\alpha$, the interaction Hamiltonian can be written as

$$\hat{H}_{int} = -\frac{\varepsilon^2(\tau)}{4}\frac{\Delta\alpha}{E_{tor}}[1 - \cos\beta + 2\cos\beta\cos^2\chi]. \tag{6}$$

If the pulse is sufficiently short that the molecules do not rotate during the interaction, the total wavefunction after the interaction can be written as[30]

$$|\Psi(0^+)\rangle = e^{iP(1-\cos\beta+2\cos\beta\cos^2\chi)}|\Psi(0)\rangle, \tag{7}$$

where

$$P = \frac{1}{4}\frac{\Delta\alpha}{E_{tor}}\int\varepsilon^2(\tau)d\tau \tag{8}$$

is the effective interaction strength and $|\Psi(0)\rangle$ is the wavefunction before the interaction. If the molecule is initially in its ground rotational and torsional state

$$|\Psi(0)\rangle = \left|\phi_0^{tor}\right\rangle\left|\phi_0^{rot}\right\rangle, \tag{9}$$

the wavefunction at the end of the pulse is expanded in a basis of eigenfunctions of the molecular Hamiltonian of Eq. (2) as

$$|\Psi(0^+)\rangle = \sum_{n=0}^{\infty}\sum_{k=-\infty}^{\infty} c_{n,k}\left|\phi_n^{tor}\right\rangle\left|\phi_k^{rot}\right\rangle. \tag{10}$$

After the interaction the system evolves freely and

$$|\Psi(\tau)\rangle = \sum_{n=0}^{\infty}\sum_{k=-\infty}^{\infty} c_{n,k}e^{-iE_{n,k}\tau}\left|\phi_n^{tor}\right\rangle\left|\phi_k^{rot}\right\rangle, \tag{11}$$

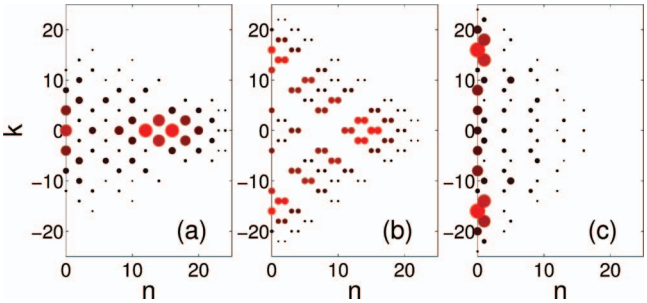

FIG. 2. Excited torsional (n) and rotational (k) eigenstates after interaction with a short laser pulse. The absolute square $|c_{n,k}|^2$ of the expansion coefficients is shown, where the diameter of the circles is proportional to $|c_{n,k}|^2$. The effective interaction strength is $P = 10$. Panel (a): initially twisted molecule ($V_0 = 10$), panel (b): no torsional potential ($V_0 = 0$), panel (c): initially planar molecule ($V_0 = -10$). Here, V_0 is given in units of E_{tor}.

where the energy eigenvalues of the field-free system are given by $E_{n,k} = E_n^{tor} + E_k^{rot}$. For a molecule which is initially in its ground rotational and torsional state, the coefficients $c_{n,k}$ can be written as

$$c_{n,2k} = i^k \exp(i P) \int_0^{2\pi} d\beta \, \phi_n^{tor\,*}(\beta) \phi_0^{tor}(\beta) J_k(P \cos\beta) \tag{12}$$

and

$$c_{n,2k+1} = 0, \tag{13}$$

where J_k is a Bessel function of kth order. Figure 2 shows the distribution of rotational and torsional states that are excited by a short laser pulse with an effective interaction strength $P = 10$. In panel (a), the potential barrier is $V_0 = 10$, i.e., the potential minima are at $\beta = \pi/2$ and $\beta = 3\pi/2$ and the molecule is initially twisted. In this case, the laser pulse mainly excites torsional states and overall rotation is hindered by the twisted geometry. A potential barrier of $V_0 = -10$ (panel (c)) corresponds to an initially planar molecule. Here, mainly rotational states are excited; since both rotors are affected by the interaction in the same way, basically no internal torsion is induced. An intermediate case is shown in panel (b), where $V_0 = 0$. For systems that exhibit negligible torsional barrier, the torsional motion is initially isotropic. As a consequence, both torsional and rotational states are excited by the laser pulse.

The subsequent rotational-torsional dynamics can be quantified in terms of similar expectation values to those used in the past in the context of alignment[1] and torsional alignment.[17] Specifically, we define a torsional alignment factor as

$$A^{tor}(\tau) = \langle \cos^2\beta \rangle(\tau) = \langle \Psi(\tau) | \cos^2\beta | \Psi(\tau) \rangle \, . \tag{14}$$

If the two moieties of the molecule are coplanar, $A^{tor} = 1$, if they are twisted by 90°, the torsional alignment factor is zero. In the limit of an isotropic distribution, where all torsion angles $0 \le \beta \le 2\pi$ are equally probable, $A^{tor} = 0.5$. Below we will find it useful to introduce measures of the individual moieties alignment with respect to the second pulse polarization vector as

$$A^{(j)}(\tau) = \langle \cos^2 \chi_j \rangle(\tau). \tag{15}$$

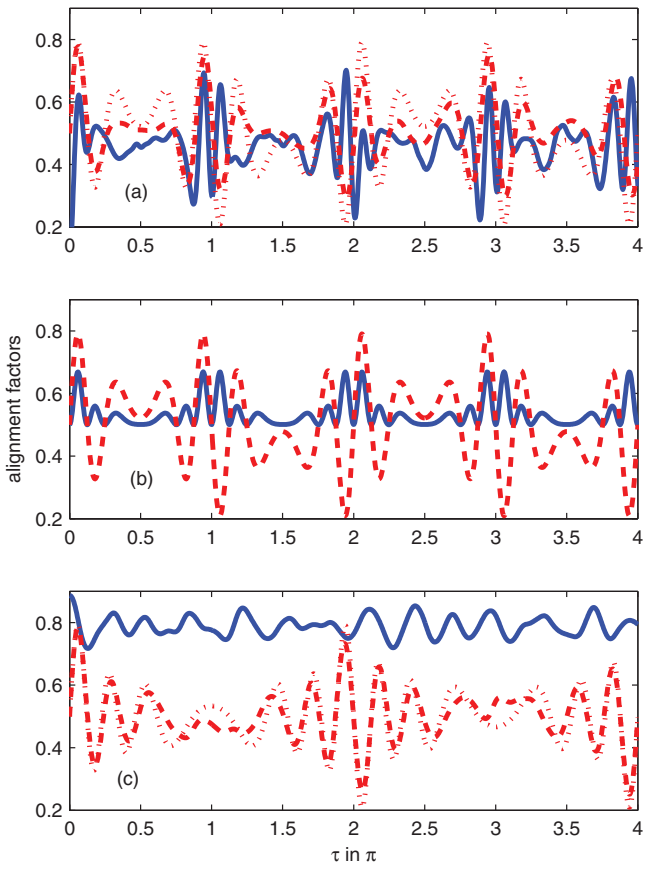

FIG. 3. Alignment factors $A^{tor}(\tau)$ (blue curves) and $A^{(1)}(\tau) = A^{(2)}(\tau)$ (dashed red curves) after interaction with a strong, non-resonant laser pulse. The effective interaction strength is $P = 10$. The potential barrier is $V_0 = 10$ (twisted molecule, panel (a)), $V_0 = 0$ (panel (b)), and $V_0 = -10$ (planar molecule, panel (c)), where V_0 is given in units of E_{tor}.

The alignment factors for the three cases described above are shown in Fig. 3: Panel (a) shows the alignment factors of an initially twisted molecule ($V_0 = 10$, as in Fig. 2(a)). Before the interaction ($\tau = 0$), the torsional alignment factor is $A^{tor} \approx 0.11$, corresponding to a twisted configuration. The torsional wavepacket which is created by the laser pulse leads to an increase of the torsional alignment. Due to the potential barrier V_0, the torsional spectrum is not quadratic in the quantum number n. As a consequence, $A^{tor}(\tau)$ does not show exact revivals. Nevertheless, quasi-revivals and quasi-fractional revivals of the rotational dynamics at $\tau \approx \pi$, 2π, etc., lead to an increase of the torsional alignment factor to $A^{tor} \approx 0.7$. This demonstrates that twisted molecules can be forced to the coplanar configuration at specific times by strong, non-resonant laser pulses, as was demonstrated earlier in Refs. 17 and 18. The alignment of the individual parts of the molecule with respect to the laser field is similar to the alignment of a single planar rotor with $I = I_j$ (see dotted curve). Due to the potential barrier, the maximal alignment is slightly reduced compared to a free rigid rotor. The alignment of an initially planar molecule ($V_0 = -10$) is shown in Fig. 3(c). Here, the torsional alignment factor, $A^{tor} \approx 0.9$, is high at $\tau = 0$. Since the laser pulse excites almost no higher torsional states (see

Fig. 2(c)), the torsional alignment is barely affected by the laser pulse, the molecules remain in an almost planar geometry. The alignment factor of the individual moieties of the molecule shows the first revival of the initial alignment at $\tau \approx 2\pi$, illustrating that a coherent torsional wavepacket behaves similar to a wavepacket of linear rigid rotor eigenstates, with a moment of inertia $I_{tot} = 2I_j$ (dotted curve). The intermediate case, $V_0 = 0$, is considered in Fig. 3(b). In this case, the alignment factors can be calculated analytically since the motion of the two rotors is decoupled and

$$|\Psi(\tau)\rangle = |\Psi^{(1)}(\tau)\rangle|\Psi^{(2)}(\tau)\rangle. \tag{16}$$

The alignment factor for the individual rotors can then be written as

$$A^{(j)} = \langle \cos^2 \chi_j \rangle = \frac{1}{2}(1 + Re\langle \exp(i2\chi_j)\rangle)$$
$$= \frac{1}{2}(1 + \cos(k_{j0}\tau) J_1 [P \sin(\tau)]), \tag{17}$$

where J_1 is a Bessel function of first order. The derivation of Eq. (17) is provided in Appendix A. In Eq. (17), the initial state is an arbitrary rotational eigenstate

$$\phi^{(j)}_{k_{j0}}(\chi_j) = \frac{1}{\sqrt{2\pi}} \exp(ik_{j0}\chi_j). \tag{18}$$

The torsional alignment factor can be expressed as

$$A^{tor} = \langle \cos^2 \beta \rangle = \langle \cos^2(\chi_1 - \chi_2)\rangle$$
$$= \frac{1}{2}\left(1 + Re\left\{\langle \exp(i2\chi_1)\rangle \langle \exp(i2\chi_2)\rangle\right\}\right). \tag{19}$$

Inserting Eq. (A7), one obtains that

$$A^{tor} = \frac{1}{2}\left(1 + \cos[(k_{10} - k_{20})\tau] J_1^2 [P \sin(\tau)]\right). \tag{20}$$

In Fig. 3(b), we assume that the molecules are in their rotational and torsional ground state, corresponding to $k_{10} = k_{20} = 0$. The dynamics of a thermal ensemble will be discussed in Sec. III. The initial value of both alignment factors is 1/2, reflecting the isotropic distribution of torsion and rotation angles. Without torsional barrier, the rotational-torsional dynamics is exactly periodic, the alignment factor $A^{(j)}(\tau)$ is repeated at multiples of $\tau_{rev} = 2\pi$. Whenever the two parts of the molecule are aligned in the direction of the laser field ($A^{(j)} \approx 0.8$) or perpendicular to it ($A^{(j)} \approx 0.2$), the torsional alignment is increased because the two moieties of the molecule are coplanar.

We conclude this section by exploring the maximal degree of torsional alignment that can be achieved for a given torsional potential as a function of the interaction strength P. Figure 4 shows the maximal torsional alignment after excitation with a single laser pulse for torsional potentials ranging from $V_0 = -100$ to $V_0 = 100$. As we have seen before, planar molecules with a relatively high barrier for torsion (solid and dashed blue curves in Fig. 4) have intrinsically a high internal alignment which is barely affected by a laser pulse, independent of the interaction strength. The torsional alignment of twisted molecules (solid and dashed red curves) rises with increasing interaction strength. For $V_0 = 0$ (black line in Fig. 4), the maximal alignment increases monotonously until A^{tor} = 0.69. The torsional alignment factor $A^{tor} = [1 + J_1^2(x)]/2$ has its maximum at $x = P \sin\tau = \pm 1.85$. The maximal degree of internal alignment can, therefore, be achieved with the effective interaction strength $P = 1.85$, any further increase of P does not influence the maximal degree of alignment. An interesting behavior is observed for small but non-zero potential barriers (dashed-dotted curves in Fig. 4), where the maximal alignment does not increase monotonously with the interaction strength. Certain values of P, i.e., certain pulse strengths, are preferable for effective internal alignment. Note, moreover, that twisted molecules with a very low barrier (dashed-dotted red curve) can have a larger degree of torsional alignment than molecules with no potential barrier at all.

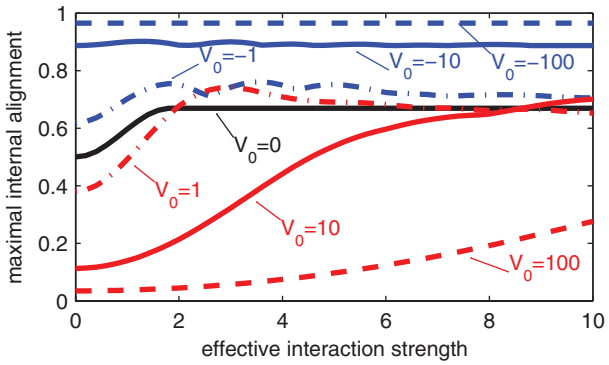

FIG. 4. Maximal degree of torsional alignment vs the interaction strength P. Here, $V_0 = 0$ (black curve), $V_0 = 1$, 10, and 100 (dashed-dotted, solid, and dashed red curves, respectively) and $V_0 = -1$, -10, and -100 (dashed-dotted, solid, and dashed blue curves, respectively), where V_0 is given in units of E_{tor}.

III. NUCLEAR SPIN SELECTIVE TORSIONAL ALIGNMENT

Molecules containing identical nuclei exist in isomeric forms called nuclear spin isomers. They are a direct consequence of the symmetrization postulate, which determines the symmetry of the total molecular wavefunction $\psi^{mol} = \psi^{spa} \cdot \psi^{nu.sp}$ and thus allows only specific symmetry combinations of spatial wavefunctions in the electronic ground state ψ^{spa} and nuclear spin states $\psi^{nu.sp}$. It has been demonstrated[11,13,14] that the alignment of rigid molecules is nuclear spin selective. In the following, we discuss how torsional molecular alignment of a non-rigid rotor depends on its nuclear spin. As an example, we consider diboron tetrafluoride B_2F_4, which exhibits torsion in the electronic ground state, as shown by gas phase infrared spectroscopy.[24] As before, we assume that the molecules are prealigned along the space-fixed z axis (see Fig. 1). It is shown in Appendix B that the total molecular wavefunction ψ^{mol} of adiabatically aligned B_2F_4 transforms according to the irreducible representation A_2 of the permutation group $G_4 = \{E, (12), (34), (12)(34)\}$. Here, (12) and (34) denote the permutation of nuclei 1 with 2 and 3 with 4, respectively. The labeling of the identical nuclei is shown in Fig. 5, and the irreducible representations of G_4 are given in the character table (see Table I). B_2F_4 exists in the form of four nuclear spin isomers denoted by $\Gamma^{spa}[\Gamma^{nu.sp}]$,

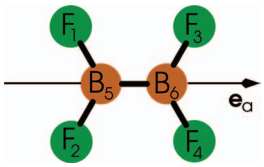

FIG. 5. Reference structure of B_2F_4, showing the labeling of the nuclei.

where Γ^{spa} and $\Gamma^{nu.sp}$ stand for the irreducible representations of spatial and nuclear spin wavefunctions. The four nuclear spin isomers are

$$A_1[A_2], \quad A_2[A_1], \quad B_1[B_2], \quad \text{and} \quad B_2[B_1]. \tag{21}$$

The potential barrier for B_2F_4 is $|V_0| \approx 0.02$ eV $= 118E_{tor}$.[25] Such barrier leads to a high degree of alignment of the lowest torsional eigenstate, as seen in Fig. 4. At higher initial temperature, the torsional wavefunctions are less localized and show a smaller degree of torsional alignment; their behavior approaches unhindered torsion as the thermal torsional energy exceeds the barrier height. In the following, we therefore assume that $V_0 = 0$ in order to keep the expressions simple and transparent. The spatial eigenfunctions can then be written as a product of eigenfunctions of the individual rotors

$$\phi_{k_1,k_2}(\chi_1, \chi_2) = \phi_{k_1}(\chi_1)\phi_{k_2}(\chi_2) = \frac{1}{2\pi}\exp(ik_1\chi_1)\exp(ik_2\chi_2) \tag{22}$$

with the energy eigenvalues

$$E_{k_1,k_2} = \frac{1}{4}\left(k_1^2 + k_2^2\right). \tag{23}$$

The symmetry of the nuclear spin state determines which combinations of k_1 and k_2 are allowed: The nuclear spin isomer $A_1[A_2]$ has only states with k_1 = even and k_2 = even; for isomer $A_2[A_1]$ only odd values of k_1 and k_2 are allowed; and for the isomers $B_1[B_2]$ and $B_2[B_1]$, k_1 is even and k_2 is odd, and vice versa. The energy eigenvalues of the four nuclear spin isomers are shown in Fig. 6. Although the symmetrization postulate allows for four different nuclear spin isomers, only three of them can be distinguished according to their energies; the two B-isomers are degenerate. The torsional alignment factors of a system that is initially in an eigenstate with the quantum numbers k_{10} and k_{20} are given by Eqs. (17) and (20). Averaged over an initially thermal ensemble of molecules at temperature T, the alignment factor of

TABLE I. The character table of the group G_4 together with the transformation properties of the angles χ_1 and χ_2 under the the permutations of G_4.

G_4	E	(12)	(34)	(12)(34)
χ_1	χ_1	$\chi_1 + \pi$	χ_1	$\chi_1 + \pi$
χ_2	χ_2	χ_2	$\chi_2 + \pi$	$\chi_2 + \pi$
A_1	1	1	1	1
A_2	1	−1	−1	1
B_1	1	−1	1	−1
B_2	1	1	−1	−1

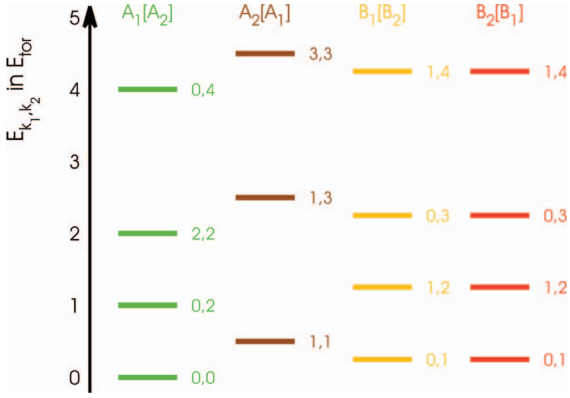

FIG. 6. Energy levels E_{k_1,k_2} for the four nuclear spin isomers of diboron tetrafluoride. The energy is given in units of E_{tor} and the nuclear spin isomers are denoted by $\Gamma^{spa}[\Gamma^{nu.sp}]$.

each isomer is given by

$$\langle\langle\cos^2\zeta\rangle\rangle = \sum_{k_{10},k_{20}\in\Gamma} \frac{\exp\left(-\frac{E_{k_{10},k_{20}}}{k_BT}\right)}{Q^\Gamma}\langle\cos^2\zeta\rangle_{k_{10},k_{20}}, \tag{24}$$

where Q^Γ is the Maxwell-Boltzmann partition function. The summation contains only those k_{j0} that are allowed for a given isomer. The angle ζ is either the torsional angle β or one of the rotation angles χ_j of the individual rotors. An ensemble of B_2F_4 molecules contains all four nuclear spin isomers, each weighted by a function that depends on the corresponding torsional eigenvalue and spin statistics, as shown in Appendix B in Eq. (B5).

The alignment factors $A^{(j)}(\tau)$ and $A^{tor}(\tau)$ for a thermal ensemble of B_2F_4 molecules with the initial temperature $T = 1$ K are shown in Fig. 7 as red and blue curves, respectively. For B_2F_4, the effective interaction strength $P = 10$ can be obtained, for instance, with a laser pulse with a duration of 100 fs and an intensity of 8×10^{12} W/cm^2. At $T = 1$K, only the ground state of each isomer (see Fig. 6) is populated initially. Immediately after the interaction ($\tau \approx 0$) and close to the revival time $\tau_{rev} = 2\pi$, we observe essentially the same behavior as discussed in the context of Fig. 3(b). Between revivals, however, the structures observed in Fig. 3(b) are washed out. In particular, no torsional alignment is observed at $\tau \approx \pi$ and $\tau \approx 3\pi$, contrary to the observations of Fig. 3(b). The origin of the difference is readily understood by considering the alignment factors of

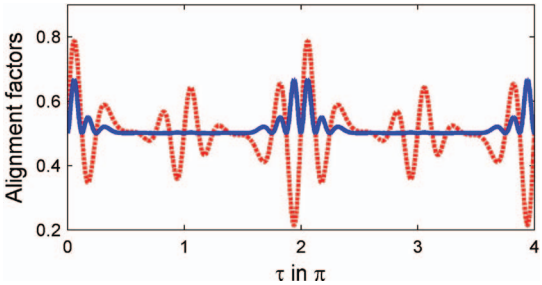

FIG. 7. Torsional alignment factors $A^{tor}(\tau)$ (blue curve) and $A^{(1)}(\tau) = A^{(2)}(\tau)$ (dashed red curve) for a thermal ensemble of B_2F_4 at T = 1 K and P = 10.

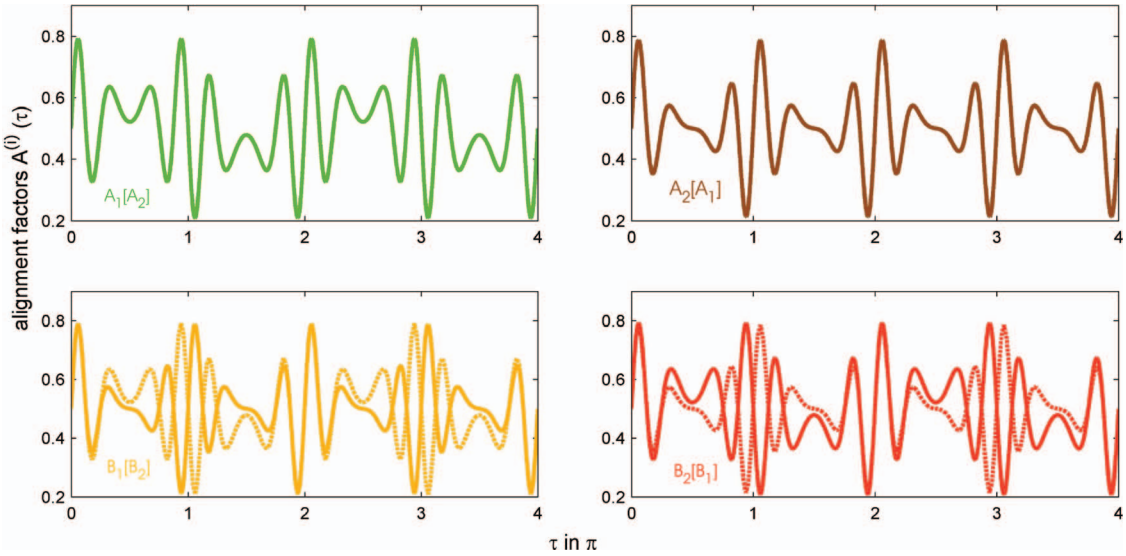

FIG. 8. Alignment factors $A^{(1)}(\tau)$ (solid curves) and $A^{(2)}(\tau)$ (dashed curves) for the four nuclear spin isomers of B_2F_4 for T = 1 K and P = 10. The isomers $A_1[A_2]$ and $A_2[A_1]$ are shown in green and brown curves, isomer $B_1[B_2]$ is depicted in yellow and isomer $B_2[B_1]$ in red.

the four individual nuclear spin isomers, Figs. 8 and 9. Figure 8 shows the alignment of the two BF_2-groups with respect to the space-fixed x axis for the four nuclear spin isomers. Immediately after the interaction, all four isomers show the same rotational dynamics; the alignment of both molecular moieties increases from a uniform distribution ($A^{(j)} = 0.5$) to $A^{(j)} = 0.69$. This pattern is reconstructed at $\tau \approx 2\pi$. At $\tau \approx \pi$ however, different nuclear spin isomers behave differently. First, for the isomers $A_1[A_2]$ (green curve) and $A_2[A_1]$ (brown curve), the alignment factors $A^{(1)}(\tau)$ and $A^{(2)}(\tau)$, Eq. (17), are identical for all τ since their initial states are $k_{10} = k_{20} = 0$ and $k_{10} = k_{20} = 1$, respectively. At $\tau = 0.88\pi$, the alignment factors $A^{(j)}$ are maximal for the $A_1[A_2]$ isomer and minimal for the $A_2[A_1]$ isomer. In other words, for one isomer, both BF_2-groups are aligned along the space-fixed x axis, whereas for the other isomer, both BF_2-groups are aligned along the y axis. For the two B-isomers (yellow and red curves in Fig. 8), the two BF_2-groups have different initial states with $k_{10} = 0$ and $k_{20} = 1$ and vice versa. For isomer $B_1[B_2]$, one rotor (solid curve) is initially in state $k_{10} = 0$, whereas the other (dashed curves) is in state $k_{20} = 1$. As a consequence, one rotor is aligned along the space-fixed x axis at $\tau = 0.88\pi$, whereas the other is aligned perpendicular to it. Finally, for isomer $B_2[B_1]$ (solid and dashed red curves), one rotor is aligned along the y axis and the second along the x axis. Thus, at $\tau = 0.88\pi$, the molecules are predominantly twisted. This behavior is also reflected in the torsional alignment factor, as shown in Fig. 9. All isomers show an increase of the torsional alignment at $\tau = 0.12\pi$ and $\tau = 2.12\pi$. At $\tau = 0.88\pi$ and $\tau = 1.2\pi$, the isomers $A_1[A_2]$ and $A_2[A_1]$ (green and brown curves) are also internally aligned. For the other two isomers, A^{tor} decreases below 0.5 at $\tau = 0.88\pi$ and

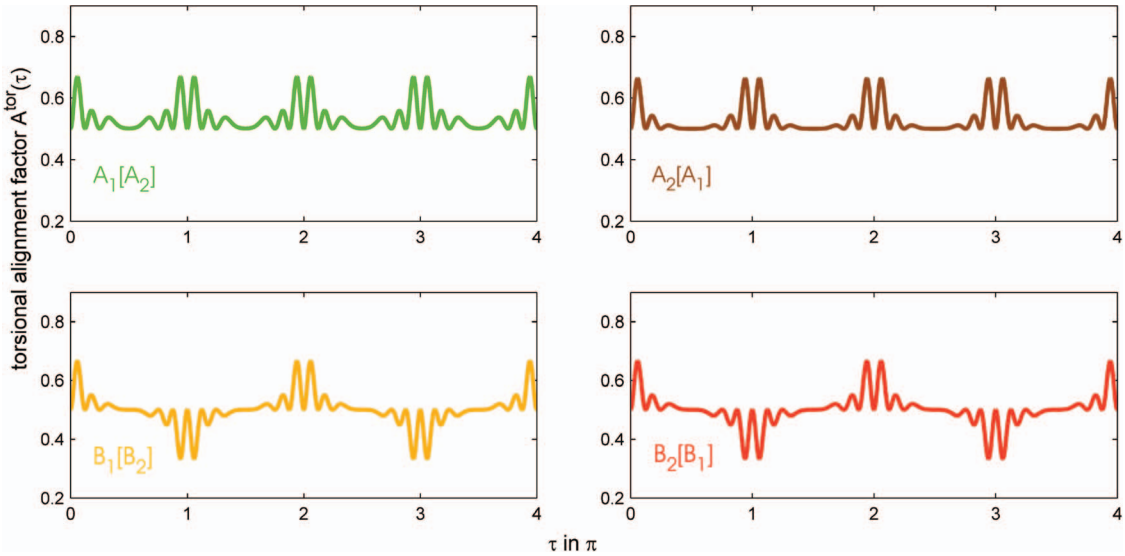

FIG. 9. Torsional alignment factor $A^{tor}(\tau)$ for the four nuclear spin isomers of B_2F_4 for T = 1 K and P = 10. The isomers $A_1[A_2]$ and $A_2[A_1]$ are shown in green and brown curves, isomer $B_1[B_2]$ is depicted in yellow and isomer $B_2[B_1]$ in red.

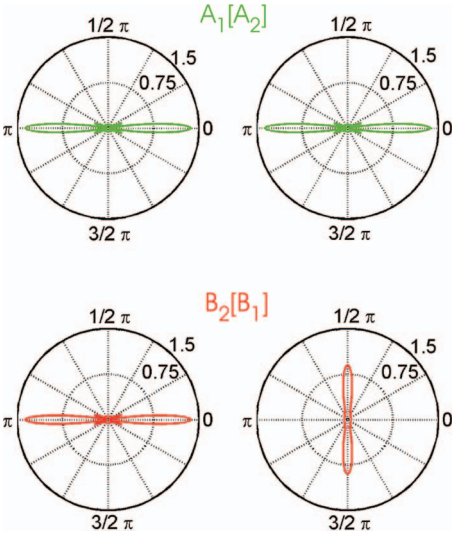

FIG. 10. Polar plot of the probability densities $|\Psi^{(j)}|^2$ for each BF_2-group at $\tau = 0.88\pi$. The probabilities $|\Psi^{(1)}(\chi_1)|^2$ and $|\Psi^{(2)}(\chi_2)|^2$ are shown in the left and right panels, respectively. The green curves (upper panel) represent isomer $A_1[A_2]$ and the red curves (lower panel) show isomer $B_2[B_1]$.

1.2π, i.e., they have a twisted transient structure. Here, we see the interesting phenomenon that, at specific times, in a sample of rotating B_2F_4 molecules, a subset of the molecules has a planar geometry, whereas other molecules are mostly twisted. This can also be seen in Fig. 10, which shows, as an example, the probability density of isomer $A_1[A_2]$ (upper panel, in green) and of isomer $B_2[B_1]$ (lower panel, in red) at $\tau = 0.88\pi$. Both BF_2-groups of isomer $A_1[A_2]$ point in the x-direction. The probability for the molecule to be planar is thus high. Isomer $B_2[B_1]$ has one BF_2-group which points in the x-direction, while the other points in the y-directions: the molecule is predominantly twisted. The torsional dynamics of those non-rigid molecules is thus highly nuclear spin selective.

IV. NUCLEAR SPIN SELECTIVE CONTROL OF ANGULAR MOMENTA

In this section, we show how the transient difference in the torsional dynamics illustrated above can be transformed into permanent, nuclear spin selective angular momenta. Earlier research has demonstrated the possibility of using a combination of two time-delayed laser pulses with different polarization to induce uni-directional rotation of rigid molecules about a molecular axis.[2–6] In this section, we extend this concept to non-rigid rotors. As in Sec. III, the system is subjected to a short x-polarized laser pulse at time $\tau = 0$ that excites rotational-torsional wavepackets. At time $\tau = \tau_2$ a second short laser pulse with different polarization direction interacts with the molecules. If we assume that the torsional barrier is negligible, i.e., set $V_0 = 0$, the wavefunction is separable, $|\Psi(\tau)\rangle = |\Psi^{(1)}(\tau)\rangle|\Psi^{(2)}(\tau)\rangle$. After the interaction, the wavefunctions for the rotor j are given by

$$|\Psi^{(j)}(\tau_2^+)\rangle = \exp[i P_2 \cos^2(\chi_j - \chi_0)]|\Psi^{(j)}(\tau_2)\rangle, \tag{25}$$

where P_2 is the effective interaction strength of the second pulse, $|\Psi^{(j)}(\tau_2)\rangle$ is the wavepacket immediately before the interaction, and χ_0 is the angle between the polarization directions of the two laser pulses. The wavepackets evolve freely after the interaction, and their angular momenta are constants. It is, therefore, sufficient to evaluate the angular momenta at $\tau = \tau_2^+$. The average angular momentum of an individual planar rotor is

$$\langle \hat{l}_z^{(j)} \rangle = -i\hbar \langle \Psi_j(\tau_2^+)| \frac{\partial}{\partial \chi_j} |\Psi_j(\tau_2^+)\rangle, \tag{26}$$

from which, using Eq. (25), one obtains

$$\begin{aligned} \langle \hat{l}_z^{(j)} \rangle &= \hbar P_2 [\sin(2\chi_0)\, \mathcal{R}e\langle \exp(i2\chi_j)\rangle \\ &\quad - \cos(2\chi_0)\, \mathcal{I}m\langle \exp(i2\chi_j)\rangle] \\ &= \hbar P_2 J_1[P \sin(\tau_2)]\{\sin(2\chi_0)\cos(k_{j0}\tau_2) \\ &\quad - \cos(2\chi_0)\sin(k_{j0}\tau_2)\}. \end{aligned} \tag{27}$$

Two other interesting observables are the torsional angular momentum

$$\langle \hat{l}_z^{tor} \rangle = -i\hbar \langle \Psi(\tau_2^+)| \frac{\partial}{\partial \beta} |\Psi(\tau_2^+)\rangle = \frac{1}{2}\left(\langle \hat{l}_z^{(1)} \rangle - \langle \hat{l}_z^{(2)} \rangle\right) \tag{28}$$

and the overall z-component of the angular momentum

$$\langle \hat{l}_z^{rot} \rangle = -i\hbar \langle \Psi(\tau_2^+)| \frac{\partial}{\partial \chi} |\Psi(\tau_2^+)\rangle = \langle \hat{l}_z^{(1)} \rangle + \langle \hat{l}_z^{(2)} \rangle. \tag{29}$$

Note that, for the model employed here and described by the Hamiltonian of Eq. (2), the angular momentum l_z^{rot} is always conserved under field-free conditions. The expectation value of the torsional angular momentum is only time-independent if the torsional potential $V(\beta)$ is neglected. For the specific case $\chi_0 = \pi/4$, we have

$$\begin{aligned} \langle \hat{l}_z^{tor} \rangle &= \hbar P_2 [\langle \cos^2 \chi_1 \rangle(\tau_2) - \langle \cos^2 \chi_2 \rangle(\tau_2)] \\ &= \hbar P_2 [A^{(1)}(\tau_2) - A^{(2)}(\tau_2)] \end{aligned} \tag{30}$$

and

$$\begin{aligned} \langle \hat{l}_z^{rot} \rangle &= 2\hbar P_2 [\langle \cos^2 \chi_1 \rangle(\tau_2) + \langle \cos^2 \chi_2 \rangle(\tau_2) - 1] \\ &= 2\hbar P_2 [A^{(1)}(\tau_2) + A^{(2)}(\tau_2) - 1]. \end{aligned} \tag{31}$$

The torsional and rotational angular momenta are thus completely determined by the degree of torsional alignment at the interaction time τ_2. Equations (30) and (31) show that the expectation values of the angular momenta are proportional to the effective interaction strength of the second pulse, P_2. Figure 11 depicts the rotational (solid curves) and torsional (dashed curves) angular momenta as functions of the delay time τ_2 for the four nuclear spin isomers of B_2F_4, averaged over an ensemble of molecules initially at a temperature $T = 1$ K. For the isomers $A_1[A_2]$ (green curves) and $A_2[A_1]$ (brown curves), the torsional angular momentum is always zero since both moieties of the molecule gain the same angular momentum, i.e., $\langle \hat{l}_z^{(1)} \rangle \equiv \langle \hat{l}_z^{(2)} \rangle$. The rotational angular momentum is determined by the degree of alignment of the two parts of the molecule at the time of the interaction with the second pulse: at instants where the two moieties of the

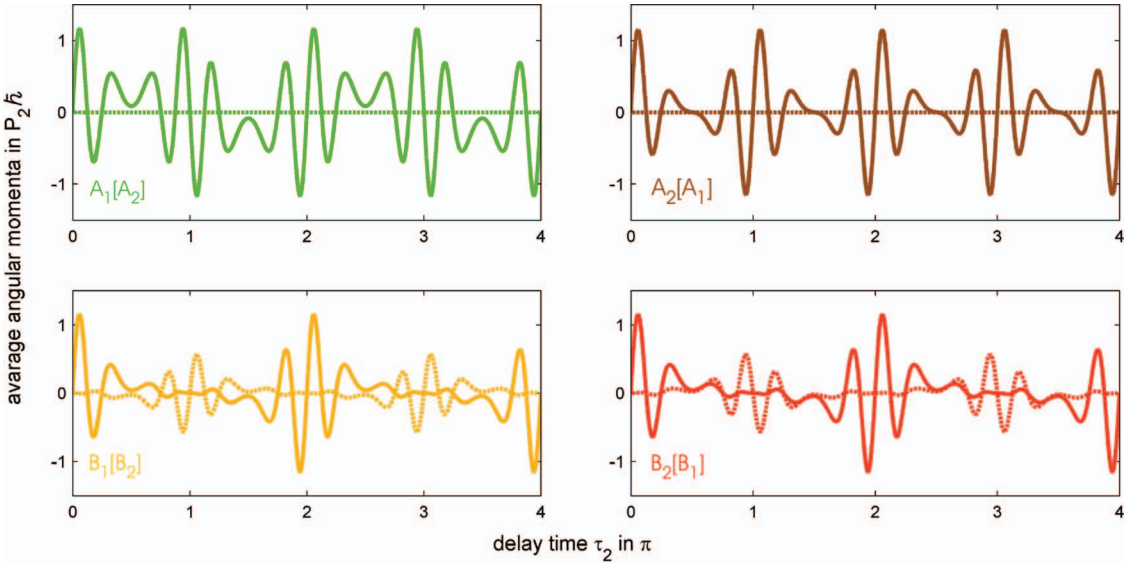

FIG. 11. Expectation value of the z-component of the angular momentum $\langle\langle \hat{l}_z^{rot}\rangle\rangle$ (solid curves) and the torsional angular momentum $\langle\langle \hat{l}_z^{tor}\rangle\rangle$ (dashed curves) in units of $\hbar P_2$ as a function of the delay time τ_2 for the four nuclear spin isomers of B_2F_4. Here, $P = 10$ and $T = 1$ K. The isomers $A_1[A_2]$ and $A_2[A_1]$ are shown in green and brown curves, isomer $B_1[B_2]$ is depicted in yellow and isomer $B_2[B_1]$ in red.

molecule are aligned with respect to the space-fixed x axis (e.g., at $\tau_2 = 0.06\pi$), the molecules gain a large amount of angular momentum – they start to spin rapidly. The sense of the rotation can be reversed by changing the delay time such that the molecules are aligned with respect to the space-fixed y axis (e.g., at $\tau_2 = 1.06\pi$). The behavior of the two B-isomers (yellow and red curves in Fig. 11) is yet more interesting. For the B-isomers, $\langle \hat{l}_z^{(1)}\rangle \neq \langle \hat{l}_z^{(2)}\rangle$ and thus, the torsional angular momentum does not vanish. Consider, for example, the delay time $\tau_2 = 0.88\pi$, where the two moieties of the B-isomers are perpendicular to each other, as shown in Fig. 10. They are thus forced by the second pulse to rotate in opposite directions and the torsional angular momentum is enhanced. At the same delay time, the two A-isomers have an enhanced rotational angular momentum. The transient differences in rotational and torsional dynamics that occur after the first pulse have thus been transformed into permanent nuclear spin selective angular momenta of the molecules. If the delay time is chosen properly, the angular momentum can be stored internally, as torsional motion for the two B-isomers and as rotational angular momentum for the A-isomers.

This effect can also be observed for the squares of the angular momenta. For the individual moieties of the molecules, they are defined as

$$\left\langle \left(\hat{l}_z^{(j)}\right)^2 \right\rangle = -\hbar^2 \langle \Psi_j(\tau_2^+)| \frac{\partial^2}{\partial \chi_j^2} |\Psi_j(\tau_2^+)\rangle, \tag{32}$$

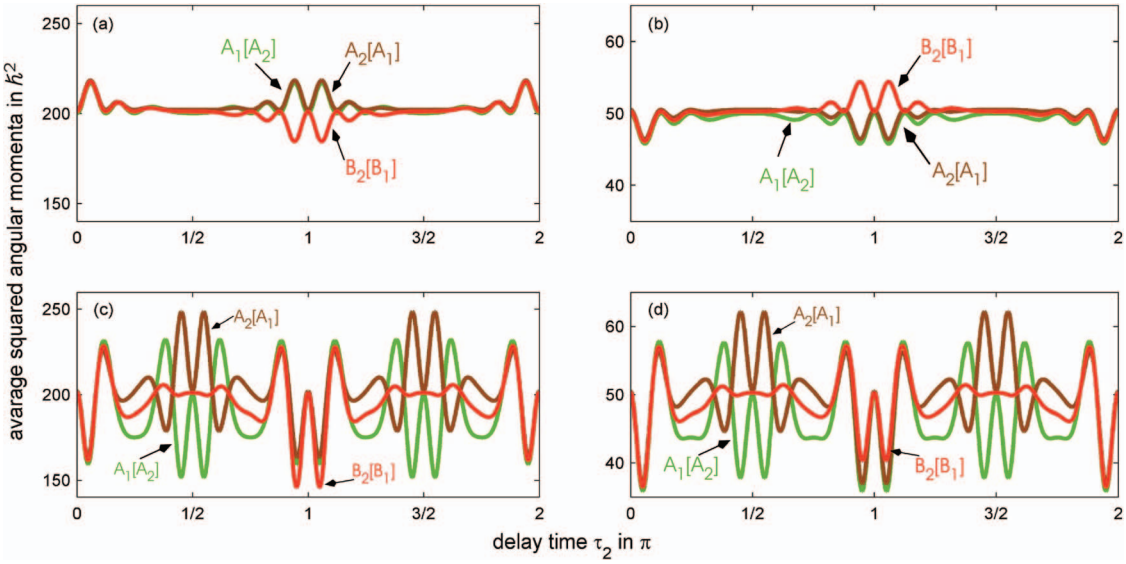

FIG. 12. Expectation values $\langle\langle(\hat{l}_z^{rot})^2\rangle\rangle$ (panels (a) and (c)) and $\langle\langle(\hat{l}_z^{tor})^2\rangle\rangle$ (panels (b) and (d)) in units of $\hbar^2$. Here, $P = P_2 = 10$ and $T = 1$ K. Panels (a) and (b) show the rotational and torsional angular momentum for $\chi_0 = \pi/4$, in panels (c) and (d), $\chi_0 = \pi/8$. The nuclear spin isomers $A_1[A_2]$ and $A_2[A_1]$ are depicted in green and brown, respectively, the $B_2[B_1]$ isomer is shown in red, its curve is identical to that of the $B_1[B_2]$ isomer.

which can be written as

$$\left\langle \left(\hat{l}_z^{(j)}\right)^2 \right\rangle = \hbar^2 \left(\frac{P^2}{2} + \frac{P_2^2}{2} + k_{j0}^2 \right) - \frac{\hbar^2 P_2^2}{2} J_2 \left[P \sin(2\tau_2) \right] \times \left[\sin(4\chi_0) \cos(2k_{j0}\tau_2) + \cos(4\chi_0) \sin(2k_{j0}\tau_2) \right]. \tag{33}$$

The expectation value $\langle(\hat{l}_z^{(j)})^2\rangle$ consists of a constant part, which is determined mainly by the effective interaction strengths P and P_2, and a part that depends on the polarization direction of the second pulse, χ_0, as well as on the delay time τ_2 between the two pulses. With the help of Eq. (33), one can also determine the square of the torsional angular momentum

$$\left\langle \left(\hat{l}_z^{tor}\right)^2 \right\rangle = -\hbar^2 \langle \Psi(\tau_2^+) | \frac{\partial^2}{\partial \beta^2} | \Psi(\tau_2^+) \rangle = \frac{1}{4} \left(\left\langle \left(\hat{l}_z^{(1)}\right)^2 \right\rangle + \left\langle \left(\hat{l}_z^{(2)}\right)^2 \right\rangle \right) - \frac{1}{2} \langle \hat{l}_z^{(1)} \rangle \langle \hat{l}_z^{(2)} \rangle \tag{34}$$

and the square of the overall angular momentum

$$\left\langle \left(\hat{l}_z^{rot}\right)^2 \right\rangle = -\hbar^2 \langle \Psi(\tau_2^+) | \frac{\partial^2}{\partial \chi^2} | \Psi(\tau_2^+) \rangle = \left(\left\langle \left(\hat{l}_z^{(1)}\right)^2 \right\rangle + \left\langle \left(\hat{l}_z^{(2)}\right)^2 \right\rangle \right) + 2 \langle \hat{l}_z^{(1)} \rangle \langle \hat{l}_z^{(2)} \rangle. \tag{35}$$

Here, we note again that the square of the torsional angular momentum is conserved only if the torsional barrier can be neglected. Both observables are shown in Fig. 12 for a thermal ensemble at temperature $T = 1$ K. Panels (a) and (b) show the expectations values $\langle\langle(\hat{l}_z^{rot})^2\rangle\rangle$ and $\langle\langle(\hat{l}_z^{tor})^2\rangle\rangle$, respectively, for $\chi_0 = \pi/4$. At a delay time of $\tau_2 = 0.88\pi$, the two A-isomers (green and brown curves) show an increase of the rotational angular momentum and a decrease of torsional angular momentum. At the same delay time, the two B-isomers (red curves) display an increase in the torsional angular momentum and a decrease in the rotational angular momentum. Thus, the squares of the angular momenta substantiate our observation and show that also energy (which is proportional to the square of the angular momentum) can be predominantly stored either in the rotational or in the torsional degrees of freedom in a nuclear spin selective manner. As seen in Fig. 6, the energy levels of the two B-isomers are degenerate and we cannot discriminate those two isomers by their rotational or torsional dynamics. The two A-isomers do have different spectra and can thus be discriminated. As shown in Figs. 12(a) and 12(b), the difference in the angular momenta of these two isomers is small for $\chi_0 = \pi/4$. Choosing $\chi_0 = \pi/8$, however (see Figs. 12(c) and 12(d)), and a delay time $\tau_2 = 0.45\pi$ or $\tau_2 = 0.55\pi$, for instance, one finds that the square of the angular momentum is maximized for the $A_2[A_1]$-isomer and minimized for the $A_1[A_2]$ isomer. In summary, with a sequence of two laser pulses with properly chosen relative polarization direction and delay time, we can nuclear spin selectively control the energy and angular momentum of the molecules.

V. CONCLUSIONS

In Secs. I–IV, we explored the possibilities of inducing and controlling the simultaneous rotational and torsional dynamics of non-rigid molecules by strong, non-resonant laser pulses, employing a model where the major molecular axis is aligned in space. We then investigated the effects of one and two short laser pulses polarized perpendicular to the aligned molecular axis. For systems with negligible torsional barrier, we derived analytical expressions for the alignment factors and the angular momenta expectation values. Our focus was the application of this approach to selective control of rotational and torsional dynamics of the nuclear spin isomers of non-rigid molecules. As an example, we considered the nuclear spin isomers of B_2F_4. We illustrated that torsional dynamics induced by a short, linear-polarized pulse depends on the nuclear spin of the system: at specific times after the pump pulse, two of the isomers of B_2F_4 have a predominantly planar structure, while the other two isomers are twisted. These transient differences in the time-dependent molecular torsion can be transformed into permanent nuclear spin selective angular momenta: a second time-delayed laser pulse with a different polarization can induce unidirectional torsion. This leads, depending on the nuclear spin, either to an increase of the overall rotation or to an enhancement of internal torsion. The energy and angular momentum of the laser pulse are thus transformed either into rotational motion of the molecules or into internal nuclear motion.

In this study, several assumptions have been made in order to keep the expressions simple and transparent. First, we assumed that the molecules are perfectly aligned – e.g., by a long, non-resonant laser pulse – throughout the investigated short-pulse-induced dynamics. Coupling between rotational and torsional degrees of freedom due to three-dimensional rotation of the molecules, which has been neglected in the present model, will effect the rotational-torsional dynamics if the alignment is not perfect. However, this effect will be reduced if a high degree of adiabatic alignment can be achieved. Second, in the simulations of nuclear spin selective rotation and torsion, we assumed that the field-free torsional barrier of the molecules is negligible. We have investigated the effects of the torsional barrier on the laser induced dynamics for molecules at very low initial temperatures in Sec. II. These effects can be reduced for higher initial temperatures of the molecules. More elaborate studies which have to include the effects of the torsional barrier and the three-dimensional rotation of the molecules will reveal these effects in detail.

The ability to selectively control rotation and torsion of nuclear spin isomers opens a variety of new and exciting opportunities. It has been demonstrated that the translational motion of molecules in non-uniform fields can be controlled by shaping the angular distribution of the molecules.[31] Since the angular distribution depends on the nuclear spin, the strategy developed above can be extended to spatially separate the nuclear spin isomers of non-rigid polyatomic molecules. Moreover, if the field energy is stored in internal nuclear motion, this may lead, depending on the strength of the interaction, to subsequent chemical reactions, such as bond-breaking. Since only particular nuclear spin isomers store the energy and angular momentum internally, these reactions will also be nuclear spin selective.

ACKNOWLEDGMENTS

We wish to thank Professor I. Sh. Averbukh (Weizmann Institute of Science), Dr. S. Fleischer (Massachusetts Institute of Technology), Professor J. Manz (Freie Universität Berlin), and Professor Y. Prior (Weizmann Institute of Science) for stimulating discussions. Financial support by the US Department of Energy (Grant No. DE-FG02-04ER15612), the German Research Foundation (LE 2138/2-1), and the Minerva Foundation is gratefully acknowledged.

APPENDIX A: ANALYTICAL EXPRESSIONS FOR THE ALIGNMENT FACTORS FOR $V_0 = 0$

If the potential barrier between the two parts of the molecule can be neglected ($V_0 = 0$), they can be treated separately as rigid rotors in a plane with the rotation angles χ_1 and χ_2. An analytical expression for the orientation of a planar rotor has been derived in Ref. 32. Here, we follow this derivation and apply it in order to calculate the alignment factor of a planar rotor which is initially in the state

$$\phi^{(j)}_{k_{j0}}(\chi_j) = \frac{1}{\sqrt{2\pi}} \exp(ik_{j0}\chi_j). \tag{A1}$$

Due to the interaction with the field, a rotational wavepacket

$$|\Psi^{(j)}(0^+)\rangle = \exp(iP\cos^2\chi_j)\left|\phi^{(j)}_{k_{j0}}\right\rangle = \sum_{k_j} c_{k_j}\left|\phi^{(j)}_{k_j}\right\rangle \tag{A2}$$

is excited. As shown in Ref. 32, the coefficients c_{k_j} can be written as

$$c_{k_j} = \left\langle\phi^{(j)}_{k_j}\right| \exp(iP\cos^2\chi_j)\left|\phi^{(j)}_{k_{j0}}\right\rangle$$

$$= \begin{cases} i^{\kappa_j}\exp\left(i\frac{P}{2}\right)J_{\kappa_j}\left(\frac{P}{2}\right) & \text{if} \quad k_j \pm k_{j0} \quad \text{even} \\ 0 & \text{if} \quad k_j \pm k_{j0} \quad \text{odd} \end{cases}, \tag{A3}$$

where $\kappa_j = (k_j + k_{j0})/2$ and J_{κ_j} is the Bessel function of order κ_j. The calculation of the alignment factors $A^{(j)}(\tau)$, Eq. (17) and $A^{tor}(\tau)$, Eq. (20) requires the evaluation of the expectation values

$$\langle\exp(i2\chi_j)\rangle = \langle\Psi^{(j)}(\tau)|\exp(i2\chi_j)|\Psi^{(j)}(\tau)\rangle \tag{A4}$$

with

$$|\Psi^{(j)}(\tau)\rangle = \sum_{k_j} c_{k_j}\exp(iE_{k_j}\tau)\left|\phi^{(j)}_{k_j}\right\rangle \tag{A5}$$

and $E_{k_j} = k_j^2/4$. Inserting expression Eq. (A3), one obtains

$$\langle\exp(i2\chi_j)\rangle = (-i)\exp(i\tau)\exp(ik_{j0}\tau) \times \sum_{k_j} J_{k_j}\left(\frac{P}{2}\right)J_{k_j+1}\left(\frac{P}{2}\right)\exp(ik_j\tau). \tag{A6}$$

Using the addition theorem for Bessel function,[33] Eq. (A6) can be simplified to

$$\langle\exp(i2\chi_j)\rangle = \exp(ik_{j0}\tau)J_1[P\sin(\tau)]. \tag{A7}$$

This expression is inserted in Eqs. (17) and (20) in order to obtain the analytical expressions for the alignment factors.

APPENDIX B: NUCLEAR SPIN ISOMERS OF B_2F_4

The molecule B_2F_4 exists in the form of different nuclear spin isomers. The symmetrization postulate states that the wavefunction of a quantum mechanical system changes its sign if two identical fermions are exchanged and remains unchanged upon the permutation of two identical bosons. In the processes considered here, the molecules remain in their electronic ground state. Since the interaction between the nuclear spin and the spatial part of the molecular wavefunction can be neglected on the time scales involved here, the total molecular wavefunction Ψ^{mol} can be written as

$$\Psi^{mol} = \Psi^{spa} \cdot \Psi^{nu.sp.}. \tag{B1}$$

The permutation symmetry of the nuclear spin state $\Psi^{nu.sp.}$ thus determines the symmetry of the spatial wavefunction. The nuclear spin isomers of a (non-rigid) molecule can be identified with the help of the permutation subgroup of the molecular symmetry (MS) group of the system.[14,34] The MS-group of diboron tetrafluoride is a G_{16}-group,[35] which has the permutation subgroup

$$G_8 = \{E, (12), (34), (12)(34), (13)(24)(56), (14)(23)(56), \times (1324)(56), (1423)(56)\}, \tag{B2}$$

where E denotes the identity (12), for example, the permutation of the nuclei 1 with 2, and (1324) means the cyclic permutation of four identical nuclei, i.e., nuclei 1 is replaced by 3, nuclei 3 is replaced by (2), nuclei 2 is replaced by 4, which is replaced by nuclei 1. The labeling of identical nuclei is shown in Fig. 5. In this study, we assume that the major molecular axis $\mathbf{e}_a$ is sharply aligned with respect to space-fixed z axis. Therefore, only the permutations (12), (34) and (12)(34) are feasible and it is sufficient to characterize the nuclear spin states according to the irreducible representations of the permutation group

$$G_4 = \{E, (12), (34), (12)(34)\}. \tag{B3}$$

It is isomorphic to the point group C_{2v} and has the character table shown in Table I. The character table also shows the effect of the symmetry operations on the angles χ_1 and χ_2 as defined in Fig. 1. Here, it is assumed that $B_2F_4 \equiv {}^{11}B_2^{19}F_4$, with nuclear spins $I_B = 3/2$ and $I_F = 1/2$, i.e., all nuclei of the molecule are fermions. Thus, under the operations of G_4 the wavefunctions Ψ^{mol} must transform according to

$$\Psi^{mol} \sim A_2. \tag{B4}$$

How the symmetry of the nuclear spin states $\psi^{nu.sp}$ can be found is described in Ref. 34. Since the group G_4 contains only permutations which interchange fluorine nuclei, the symmetry of the $2^4 = 16$ spin states of the fluorine nuclei needs to be determined. One finds that

$$\Gamma^{nu.sp} = 9A_1 \oplus 1A_2 \oplus 3B_1 \oplus 3B_2. \tag{B5}$$

The spatial eigenfunctions of B_2F_4 can be written as

$$\Psi^{spa} = \phi_{k_1,k_2}(\chi_1, \chi_2) = \frac{1}{2\pi}\exp(ik_1\chi_1)\exp(ik_2\chi_2) \tag{B6}$$

since we neglect the torsional barrier. Using the transformation properties of the two angles χ_1 and χ_2, given in Table I,

it is straightforward to verify that

$$\phi_{k_1,k_2} \sim \begin{cases} A_1 & \text{if} \quad k_1 \text{ even}, k_2 \text{ even} \\ A_2 & \text{if} \quad k_1 \text{ odd}, k_2 \text{ odd} \\ B_1 & \text{if} \quad k_1 \text{ even}, k_2 \text{ odd} \\ B_2 & \text{if} \quad k_1 \text{ odd}, k_2 \text{ even} \end{cases}. \tag{B7}$$

Since the total molecular wavefunction transforms according to A_2, one can conclude that (aligned) B_2F_4 has four nuclear spin isomers which we denote by $\Gamma^{spa}[\Gamma^{nu.sp}]$:

$$A_1[A_2], \quad A_2[A_1], \quad B_1[B_2], \quad B_2[B_1]. \tag{B8}$$

[1] T. Seideman and E. Hamilton, Adv. At. Mol. Phys. **52**, 289 (2005); H. Stapelfeldt and T. Seideman, Rev. Mod. Phys. **75**, 543 (2003).
[2] S. S. Viftrup, V. Kumarappan, S. Trippel, H. Stapelfeldt, E. Hamilton, and T. Seideman, Phys. Rev. Lett. **99**, 143602 (2007).
[3] S. S. Viftrup, V. Kumarappan, L. Holmegaard, C. Z. Bisgaard, H. Stapelfeldt, M. Artamonov, E. Hamilton, and T. Seideman, Phys. Rev. A **79**, 023404 (2009).
[4] S. Fleischer, Y. Khodorkovsky, Y. Prior, and I. Sh. Averbukh, New J. Phys. **11**, 10539 (2009).
[5] A. G. York, Opt. Exp. **17**, 23671 (2009).
[6] K. Kitano, H. Hasegawa, and Y. Ohshima, Phys. Rev. Lett. **103**, 223002 (2009).
[7] K. F. Bonhoeffer and P. Harteck, Z. Physikal. Chem. B **4**, 113 (1929).
[8] P. L. Chapovsky and L. J. F. Hermans, Annu. Rev. Phys. Chem. **315**, 315 (1999).
[9] Z. Sun, K. Takagi, and F. Matsushima, Science **310**, 1938 (2005).
[10] T. Kravchuk, M. Reznikov, P. Tichonov, N. Avidor, Y. Meir, A. Bekkerman, and G. Alexandrowicz, Science **331**, 319 (2011).
[11] S. Fleischer, I. Sh. Averbukh, and Y. Prior, Phys. Rev. Lett. **99**, 093002 (2007); J. Mod. Opt. **54**, 2641 (2007); J. Phys. B **41**, 074018 (2008).
[12] M. Renard, E. Hertz, B. Lavorel, and O. Faucher, Phys. Rev. A **69**, 043401 (2004).
[13] E. Gershnabel and I. Sh. Averbukh, Phys. Rev. A **78**, 063416 (2008).
[14] T. Grohmann and M. Leibscher, J. Chem. Phys. **134**, 204316 (2011).
[15] B. J. Sussmann, D. Townsend, M. Y. Ivanov, and A. Stolow, Science **314**, 278 (2006).
[16] J. González-Vásquez, L. González, I. R. Sola, and J. Santamaria, J. Chem. Phys. **131**, 104302 (2009).
[17] S. Ramakrishna and T. Seideman, Phys. Rev. Lett. **99**, 103001 (2007).
[18] C. B. Madsen, L. B. Madsen, S. S. Viftrup, M. P. Johansson, T. B. Poulsen, L. Holmegaard, V. Kumarappan, M. P. Jorgensen, and H. Stapelfeldt, Phys. Rev. Lett. **102**, 073007 (2009).
[19] C. B. Madsen, L. B. Madsen, S. S. Viftrup, M. P. Johansson, T. B. Poulsen, L. Holmegaard, V. Kumarappan, M. P. Jorgensen, and H. Stapelfeldt, J. Chem. Phys. **130**, 234310 (2009).
[20] S. Parker, M. Ratner, and T. Seideman, J. Chem. Phys. **135**, 224301 (2011).
[21] O. Deeb, M. Leibscher, J. Manz, W. von Muellern, and T. Seideman, ChemPhysChem **8**, 322 (2007).
[22] S. Alfalah, S. Belz, O. Deeb, M. Leibscher, J. Manz, and S. Zilberg, J. Chem. Phys. **130**, 124318 (2009); S. Belz, T. Grohmann, and M. Leibscher, *ibid.* **131**, 034305 (2009).
[23] K. Hoki, D. Kröner, and J. Manz, Chem. Phys. **267**, 59 (2001).
[24] A. Finch, I. Hyams, and D. Steele, Spectrochimica. Acta **21**, 1423 (1965).
[25] I. V. Kochinkov and Y. I. Tarasov, J. Struct. Chem. **14**, 227 (2003).
[26] R. R. Ryan and K. Hedberg, J. Chem. Phys. **50**, 4986 (1969).
[27] E. U. Condon, Phys. Rev. **31**, 891 (1928).
[28] M. Leibscher and B. Schmidt, Phys. Rev. A **80**, 012510 (2009).
[29] K. D. Bonin and V. V. Kresin, *Electric-Dipole Polarizabilities of Atoms, Molecules, and Clusters* (World Scientific, Singapore, 1997).
[30] I. Sh. Averbukh and R. Arvieu, Phys. Rev. Lett. **87**, 163601 (2001).
[31] E. Gershnabel and I. Sh. Averbukh, Phys. Rev. Lett. **104**, 152001 (2010); Phys. Rev. A **82**, 033401 (2010).
[32] M. Leibscher and I. Sh. Averbukh, Phys. Rev. A **65**, 053816 (2002).
[33] M. Abramowitz and I. A. Stegun, *Handbook of Mathematical Function* (Dover, New York, 1972).
[34] P. R. Bunker and P. Jensen, *Molecular Symmetry and Spectroscopy* (NRC Research Press, Ottawa, 1998).
[35] A. J. Merer and J. K. G. Watson, J. Mol. Spectrosc. **47**, 499 (1973).